Available online at www.sciencedirect.com
ScienceDirect
Journal of Computational Physics 227 (2008) 2626–2643
JOURNAL OF COMPUTATIONAL PHYSICS
www.elsevier.com/locate/jcp

A non-linear observer for unsteady three-dimensional flows

M. Buffoni [a], S. Camarri [b], A. Iollo [a,*], E. Lombardi [a,b], M.V. Salvetti [b]

[a] *Institut de Mathématiques de Bordeaux UMR 5251 CNRS, Université Bordeaux 1 and INRIA Futurs MC2, 351, Cours de la Libération, 33405 Talence cedex, France*
[b] *Dipartimento di Ingegneria Aerospaziale, Università di Pisa, 56122 Pisa, Italy*

Received 16 May 2007; received in revised form 26 October 2007; accepted 4 November 2007
Available online 17 November 2007

Abstract

A method is proposed to estimate the velocity field of an unsteady flow using a limited number of flow measurements. The method is based on a non-linear low-dimensional model of the flow and on an expansion of the velocity field in terms of empirical basis functions. The main idea is to impose that the coefficients of the modal expansion of the velocity field gives the best approximation of the available measurements, while at the same time satisfying the non-linear low-order model as closely as possible. Practical applications may range from feedback flow control to the monitoring of the flow in non-accessible regions. The proposed technique is applied to the flow around a confined square cylinder, both in two- and three-dimensional flow regimes. Comparisons are provided with existing linear and non-linear estimation techniques.

MSC: 65M60

PACS: 47.32.Ff; 47.50.Cd

Keywords: Low-order models; Dynamic estimation; Non-linear observer

1. Introduction

The problem of deriving an accurate estimation of the velocity field in an unsteady complex flow, starting from a limited number of measurements, is of great importance in many engineering applications. For instance, in the design of a feedback control, some knowledge of the velocity field is a fundamental element in deciding the appropriate actuator reaction to different flow conditions. In other applications it may be necessary, or advisable, to monitor the flow conditions in regions which are difficult to access, or where probes cannot be fitted without causing interference problems. Similar problems arise in physics when trying to filter data resulting from a chaotic system, see for example [1].

* Corresponding author.
E-mail address: angelo.iollo@math.u-bordeaux1.fr (A. Iollo).

0021-9991/$ - see front matter © 2007 Elsevier Inc. All rights reserved.
doi:10.1016/j.jcp.2007.11.005

The method that we propose exploits an idea which is similar to that at the basis of the Kalman filter (see [14]). The starting point is a Galerkin representation of the velocity field $\boldsymbol{u}(\boldsymbol{x},t)$ in terms of N_r empirical eigenfunctions, $\boldsymbol{\Phi}^i(\boldsymbol{x})$, obtained by proper orthogonal decomposition (POD) (see [17])

$$\boldsymbol{u}(\boldsymbol{x},t) = \bar{\boldsymbol{u}}(\boldsymbol{x}) + \sum_{i=1}^{N_r} a_i(t)\boldsymbol{\Phi}^i(\boldsymbol{x}) \tag{1}$$

where $\boldsymbol{u}(\boldsymbol{x},t) : \mathbb{R}^n \times [0,\, T] \to \mathbb{R}^n$, $\boldsymbol{\Phi}^i(\boldsymbol{x}) : \mathbb{R}^n \to \mathbb{R}^n$, $n \in \{2,3\}$ according to the physical space dimension, $\bar{\boldsymbol{u}}(\boldsymbol{x})$ is some reference velocity field and $a_i(t) :\ I = [0,T] \subset \mathbb{R} \to \mathbb{R}$.

For a given flow, the POD modes can be computed once and for all, using direct numerical simulation (DNS), or highly resolved experimental velocity fields, such as those obtained by particle image velocimetry. An instantaneous velocity field can thus be reconstructed by estimating the coefficients $a_i(t)$ of its Galerkin representation.

One simple approach to estimate the POD coefficients is to approximate the flow measurements in a least square sense, as done, for instance, in [12]. A similar procedure is also used in the estimation based on gappy POD, see [9,24,25]. Another possible approach, the linear stochastic estimation (LSE), is based on the assumption that a linear correlation exists between the flow measurements and the value of the POD modal coefficients (see, for instance, [4]).

However, these approaches encounter difficulties in giving accurate estimations when three-dimensional flows with complicated unsteady patterns are considered, or when a very limited number of sensors is available. Under these conditions, for instance, the least squares approach mentioned above (LSQ) rapidly becomes ill conditioned. This simply reflects the fact that more and more different flow configurations correspond to the same set of measurements. To circumvent these problems, many contributions in the literature have sought to determine the best sensor placement (see e.g. [20,8,7,25]). For example in [25], a systematic approach to sensor placement is formulated within the gappy POD framework using a condition number criterion.

In order to improve estimation performance, extensions of the above methods have been proposed: quadratic stochastic estimation (QSE) [2,19] and spectral linear stochastic estimation (SLSE) [10]. They allow more accurate estimations than LSQ or LSE methods, but, in fact, neither takes into account the underlying dynamic model that the POD coefficients must satisfy, i.e., a finite dimensional equivalent of the Navier–Stokes equations that is obtained by Galerkin projection of the flow equations on the POD modes retained for the representation of the velocity field.

In the literature one finds estimation techniques that take into account the underlying partial differential equations, using control theory tools [16]. Classical estimations based on such methods are those applied in meteorology where the mismatch between predictions and observations is minimized as function of the initial conditions [15]. More recent applications of these ideas are those used in seismology, where the source of an earthquake is sought once the ground displacement is measured [3]. Computing the exact solution of such inverse problems requires large computational facilities for realistic cases since the state equation, the adjoint equation and the optimality conditions must be simultaneously solved. In this sense, the novelty of the present study is to discuss an approach that combines a linear estimation of the coefficients $a_i(t)$ with an appropriate non-linear low-dimensional flow model. Compared to the classical inverse problems mentioned above, the solution is obtained with a negligible computational effort, at the cost of obtaining an approximate solution. The degree of approximation will be related to the possibility of an actual low-order representation.

The approach that we propose combines a linear estimation of the coefficients $a_i(t)$ with an appropriate non-linear low-dimensional flow model. Our objective is not, however, to propose an estimation method that can be readily implemented for real time applications, even if a few indications in this direction are given. Instead, our objective is to understand whether a non-linear observer outperforms existing linear flow observers, without the constraints imposed by an actual recursive algorithm, e.g., a real-time computation. Moreover, instead of what was done, for example, in [13], this study is confined to a deterministic framework, since the model, as well as the measurements, are supposedly not affected by noise. The measurements are not affected by noise in the sense that we do not take into account the errors introduced by the actual instruments. The model is not affected by noise in the sense that although it will only be approximate, we will not try

to mimic the model deviations by adding noise with appropriate statistical characteristics. Our results will show that, within this framework, dynamic estimations based on low-order models turn out to be more satisfactory than static approaches, i.e., those which use no model.

In addition, we address the issue of the sensitivity of the proposed approach to sensor type and location. Finally, we present an application to a flow, which is characterized by a significant three-dimensionality and non-periodic dynamics.

2. Flow set up and low-order model

The flow over an infinitely long square cylinder symmetrically confined by two parallel planes is considered. A sketch showing the geometry, the frame of reference and the adopted notation is plotted in Fig. 1. At the inlet, the incoming flow is assumed to have a Poiseuille profile with maximum center-line velocity U_c. Two Reynolds numbers $Re = U_c L/\nu$ were considered, one at which the flow is two-dimensional ($Re = 150$) and the other one leading to a three-dimensional flow in the wake ($Re = 300$). With reference to Fig. 1, $L/H = 1/8$, $L_{in}/L = 12$, $L_{out}/L = 20$ and $L_z/L = 0.6$ for the two-dimensional case, whereas $L/L_z = 6$ for the three-dimensional one. Periodic boundary conditions are imposed in the span-wise direction and no-slip conditions are enforced both on the cylinder and on the parallel walls. Details concerning the grids and the numerical set up are reported in [5]. All the quantities mentioned in the following have been made non-dimensional by L and U_c. The two-dimensional flow obtained at $Re = 150$ is a classic vortex street with a well defined shedding frequency. However, the interaction with the confining walls adds to the complexity of the flow and leads to some peculiar features, like the fact that the vertical position of the span-wise vortices is opposite to the one in the classic von Kármán street [6]. In the three-dimensional case the situation is even more complex, due to instabilities developing in the span-wise direction. The flow is no longer periodic and exhibits complicated flow patterns [5].

The POD modes $\mathbf{\Phi}^k(\boldsymbol{x})$ are found using the snapshot method [21]

$$\mathbf{\Phi}^k = \sum_{i=1}^{N} b_i^k \boldsymbol{U}^{(i)}$$

where $\boldsymbol{U}^{(i)} = \boldsymbol{u}(\boldsymbol{x}, t_i)$ are flow snapshots taken at times $t_i \in [0, T]$, N is the number of snapshots, $k \in \{1, \ldots, N\}$, and the coefficients $b_i^k \in \mathbb{R}$ are such that the vectors $(b_1^k, \ldots, b_N^k)$ are the eigenvectors of the time correlation matrix $\int_\Omega \boldsymbol{U}^{(j)} \cdot \boldsymbol{U}^{(l)}\, dx$, of size $N \times N$. Only a limited number of modes, N_r, is used to represent the velocity field. In particular we chose $N_r = 6$ for the two-dimensional case. For the three-dimensional case we derived two models with $N_r = 20$ and $N_r = 60$, respectively.

A Galerkin projection of the incompressible Navier–Stokes equations over the retained POD modes has been carried out. This leads to the following N_r-dimensional dynamical system

$$\begin{aligned} &R_r(\boldsymbol{a}(t)) = \dot{a}_r(t) - A_r - C_{kr} a_k(t) + B_{ksr} a_k(t) a_s(t) = 0 \\ &a_r(0) = (\boldsymbol{u}(\boldsymbol{x}, 0) - \bar{\boldsymbol{u}}(\boldsymbol{x}), \mathbf{\Phi}^r) \end{aligned} \tag{2}$$

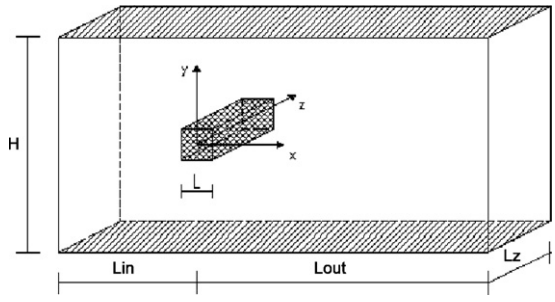

Fig. 1. Computational domain Ω.

where $\boldsymbol{a}(t) : I \to \mathbb{R}^{N_r}$ and $\boldsymbol{a}(t) = \{a_1(t), \ldots, a_{N_r}(t)\}$; r, k and s run from 1 to N_r and the Einstein summation convention is used. The scalar coefficients B_{ksr} come directly from the Galerkin projection of the non-linear terms in the Navier–Stokes equations, and they can easily be expressed in terms of the POD modes. The scalar terms A_r and C_{kr} are calibrated using a pseudo-spectral method to take into account the pressure drop, as well as the interaction of unresolved modes in the POD expansion. Indeed, we could in principle write the solution of the equation for the unresolved modes as a function of the resolved ones and then inject this solution into the equation for the resolved modes. We do not use such an explicit solution as done for example in [18], but instead, find its MacLaurin expansion up to the linear term by an optimization technique. Thus, the calibration terms that we add to the model can be interpreted as the coefficients of such an expansion.

In this paper we consider two calibration methods. The first consists in solving an inverse problem, where the coefficients A_r and C_{kr} are found in order to minimize the difference, measured in the L^2 norm, between the model prediction and the actual reference solution. See [11] for a detailed discussion of the calibration technique. The resulting model for the two-dimensional flow configuration considered here is very accurate in describing the asymptotic attractor [12,11]. For the three-dimensional case, it was shown in [5] that the calibrated model is capable of accurately reproducing the complicated flow dynamics resulting from the interaction of the three-dimensional vortex wake with the confining walls inside the calibration interval. Although very accurate, the computational cost of obtaining this model is not negligible when the number of modes is large or when the flow shows a large span of time frequencies. We denote this calibration technique by M1.

For this reason, we used an alternative method that gives a reasonable model at the cost of a matrix inversion. The idea is simple. We ask that the terms A_r and C_{kr} are such that

$$\int_0^T \dot{a}_r \,\mathrm{d}t = A_r T + C_{kr} \int_0^T a_k \,\mathrm{d}t - B_{ksr} \int_0^T a_k a_s \,\mathrm{d}t \tag{3}$$

and

$$\int_0^T \dot{a}_r a_m \,\mathrm{d}t = A_r \int_0^T a_m \,\mathrm{d}t + C_{kr} \int_0^T a_k a_m \,\mathrm{d}t - B_{ksr} \int_0^T a_k a_s a_m \,\mathrm{d}t \tag{4}$$

are satisfied $\forall r, m \in \{1, \ldots, N_r\}$. The time interval $[0, T]$ is the same as that considered for building the POD modes. Hence, all the integrals in the above equations are known and, for each r, a set of $N_r + 1$ linear equations is obtained for the coefficients A_r and C_{kr}. It can be seen that this technique amounts to a minimization of the model prediction error in the H^1 norm. We denote this technique by M2.

3. Non-linear observer

Our aim is to provide an estimation of the modal coefficients starting from N_s flow measurements $f_k, k \in \{1, \ldots, N_s\}$. Let $\bar{\alpha}_i(t)$ be the projection of the velocity field $\boldsymbol{u}(t)$ over the ith POD mode and $\alpha_i(t)$ be its estimated value at time t.

We assume that each measurement f_k is a scalar quantity which depends linearly on the instantaneous velocity field $\boldsymbol{u}(t)$. For instance, f_k can be a point-wise measurement of a velocity component, or of a shear stress, or it can be a spatial average of a linear combination of velocity components.

The available spatial information may be exploited by using a LSQ approach, as done in [12]. At any given time τ, thanks to the linearity of f_k with respect to $\boldsymbol{u}$ and to the modal decomposition of the velocity field (see Eq. (1)), f_k can be written in terms of POD modes

$$f_k(\boldsymbol{u}(\tau)) \simeq \sum_{j=1}^{N_r} a_j(\tau) f_k(\boldsymbol{\Phi}^j) \tag{5}$$

where $f_k(\boldsymbol{\Phi}^j)$ is obtained by applying f_k to the vector field associated to mode $\boldsymbol{\Phi}^j$. The following least-squares problem then has to be solved for every τ

$$\min_{\{\omega_1(\tau), \ldots, \omega_{N_r}(\tau)\}} \sum_{k=1}^{N_s} \left(f_k(\boldsymbol{u}(\tau)) - \sum_{j=1}^{N_r} \omega_j(\tau) f_k(\boldsymbol{\Phi}^j) \right)^2 \tag{6}$$

where $\omega_j(\tau)$ is an optimization variable representing the mode coefficient at time τ.

This minimization leads to a N_r-dimensional linear system of equations. Once this system is solved, the estimated modal coefficients can be written

$$\alpha_j(\tau) = \sum_{k=1}^{N_s} \Upsilon_{kj} f_k(\boldsymbol{u}(\tau)) \tag{7}$$

where Υ is a known rectangular matrix of size $N_s \times N_r$. The error minimization (6) leads to a linear representation of the estimated modes as functions of the measurements. When the number of the modes retained is larger than the number of sensors, matrix Υ is rank deficient. In such cases we opted for a Tikhonov regularization technique: among the infinite number of solutions we chose the one that minimizes the sum of the squared residuals and the norm of the solution multiplied by a small positive factor.

The LSE approach, conversely, exploits temporal rather than spatial information and is based on the assumption that a linear relation exists between the modal coefficients and the measurements

$$\alpha_j(\tau) = \sum_{k=1}^{N_s} \Lambda_{kj} f_k(\boldsymbol{u}(\tau)) \tag{8}$$

where Λ is now an unknown rectangular matrix of size $N_s \times N_r$. This matrix is determined by imposing that $\forall j \in \{1, \ldots, N_r\}$ and $\forall k \in \{1, \ldots, N_s\}$

$$\int_0^T \bar{\alpha}_j(t) f_k(\boldsymbol{u}(t))\,\mathrm{d}t = \int_0^T \sum_{m=1}^{N_s} \Lambda_{mj} f_m(\boldsymbol{u}(t)) f_k(\boldsymbol{u}(t))\,\mathrm{d}t \tag{9}$$

The time interval $[0, T]$ is the same as that considered for building the POD modes. Hence, since the left-hand side is known, a set of linear equations is obtained; these uniquely define the matrix Λ.

The LSQ and LSE both provide linear estimation of the modal coefficients. Matrices Υ and Λ have the same size, although the coefficients are different. In the following we overcome the assumption of a linear relation.

Let us assume that a certain number of measurements at consecutive times τ_m, $m \in \{1, \ldots, N_m\}$ are available. The main idea of the dynamic estimation approach proposed here is to impose that the coefficients of the modal expansion of the velocity field give the best approximation of the available measurements, using either LSQ (7) or LSE (8), and that at the same time they satisfy as closely as possible the non-linear low-order model (2).

In the LSQ case this is done by minimizing the sum of the residuals of (7) and the residuals of (2) for all times τ_m. More precisely, let $\boldsymbol{\alpha}(t) : \mathbb{R} \to \mathbb{R}^{N_r}$ and $\boldsymbol{\alpha}(t) = \{\alpha_1(t), \ldots, \alpha_{N_r}(t)\}$, we have

$$\boldsymbol{\alpha}(t) = \underset{\boldsymbol{\omega}(t)}{\operatorname{argmin}} \sum_{m=1}^{N_m} \left[\sum_{r=1}^{N_r} R_r^2(\boldsymbol{\omega}(\tau_m)) + C_{\mathrm{R}} \sum_{r=1}^{N_r} \left(\omega_r(\tau_m) - \sum_{k=1}^{N_s} \Upsilon_{kr} f_k(\boldsymbol{u}(\tau_m)) \right)^2 \right] \tag{10}$$

where $\boldsymbol{\omega}(t) = \{\omega_1(t), \ldots, \omega_{N_r}(t)\}$ is an optimization variable standing for the mode coefficients vector at time t. The parameter C_{R} is a weight, giving more or less importance to the measurements (LSQ) or to the dynamic model in the definition of the residual norm. This parameter could be replaced by a matrix that takes into account a priori information like the reliability of some of the measurements vs. others, or the model error statistics. In the numerical experiments reported here, this parameter was set in a heuristic way, leaving further developments to future investigations.

The minimization of this functional is reduced to a non-linear algebraic problem. As in [11], a pseudo-spectral approach is used and each $a_r(t)$ is expanded in time using Lagrange polynomials defined on Chebyshev–Gauss–Lobatto collocation points. The necessary conditions for the minimum are obtained by the adjoint method and they result in a non-linear set of algebraic equations for the coefficients of the Lagrange polynomials [11]. The solution is obtained by a Newton method, which, in the present applications, usually converges in a few (typically 5–8) iterations. The complexity of the method is equivalent to the complexity of any technique employed to solve a system of non-linear algebraic equations. The systems we are dealing with are usually small ($N_r \cdot N_m$ unknowns) and hence the computational time to find the solution is small. However,

the main reason that prevents us from using the present method in real time is that we need to collect the entire time history of the measurements before performing the estimation.

The solution to problem (10) provides an estimation for the POD modal coefficients for all retained modes and for all instants at which measurements are available. This enables the reconstruction of the entire flow field at the same instants through Eq. (1). The above method, therefore, represents a non-linear observer of the flow state. In the following, it will be referenced as K-LSQ.

A similar approach can be obtained for the LSE technique, by substituting, in Eq. (10), the residuals of Eq. (7) by those of Eq. (8). This approach is referenced as K-LSE.

In the literature, there exist other flow estimation techniques that are non-linear in the flow measurements. In the following we will compare the results of the proposed non-linear dynamic estimation to one of them, the quadratic extension of LSE [2,19]. LSE is based on the assumption that Eq. (8) is just the first term of a Taylor expansion with respect to the sensor measurements, whereas QSE takes into account the second order term, too. Hence, we have

$$\alpha_j(\tau) = \sum_{k=1}^{N_s} \Lambda_{kj} f_k(\boldsymbol{u}(\tau)) + \sum_{k=1}^{N_s}\sum_{m=1}^{N_s} \Omega_{kmj} f_k(\boldsymbol{u}(\tau)) f_m(\boldsymbol{u}(\tau)) \tag{11}$$

where the scalar coefficients Λ_{kj} and Ω_{kmj} are obtained using double, triple and quadruple correlations between measurements in an equation equivalent to (9). This approach is referred to as QSE.

Once the matrices appearing in Eqs. (7), (8) and (11) are computed, the estimation of the modal coefficients at a certain time is based on the measurements made at the same time.

In contrast, Ewing and Citriniti [10] and Tinney et al. [23] proposed to take into account integrated temporal data by assuming a linear dependence between the modal coefficients and the flow measurements in a non-local way, and working in the frequency domain. Let $\hat{\alpha}$ be the Fourier transform of α and $\hat{f}_j$ that of f_j, then for each frequency we set

$$\hat{\alpha}_j = \sum_{k=1}^{N_s} \widehat{\Gamma}_{kj} \hat{f}_k \tag{12}$$

where $\widehat{\Gamma}_{kj}$ is a matrix obtained by appropriate ensemble averages and depends on the frequency. In the time domain this amounts to a convolution integral between the measurements and the time dependent matrix Γ. We call this approach SLSE. As compared to QSE and SLSE, the dynamic estimation procedure that we propose is non-linear and, at the same time, it takes into account the evolution of the modal coefficients in time by constraining such evolution to a model, in the weak sense determined by Eq. (10).

Concerning the applicability of the methods described above, it is important to recall that the LSE and LSQ approaches are readily applicable to real-time estimation, QSE also, although the cost of this last approach scales as N_s^2 instead of linearly as in the previous two cases. Conversely, the SLSE approach is more difficult to use for real-time estimations, since it uses the whole temporal history of the measurements, collected in a time interval, coupled together (linearly) via the discrete Fourier transform (DFT). This implies that the estimation problem must be tackled after having collected enough temporal information and it consists of a number of LSE problems equal to the number of retained frequencies, plus additional DFT's of the measurements and of the estimated POD coefficients. Similarly to what was done in the SLSE approach, in the present dynamic estimations the temporal histories of the measurements are coupled together (non-linearly) by the dynamic POD model. This aspect poses difficulties in a real-time application. Indeed, as pointed out in the introduction, K-LSQ or K-LSE are thought to be applied a-posteriori, because their computational cost, although unimportant in a post-processing phase, is large for a real-time analysis. Nevertheless, although actual real-time applications are premature, a proposal for their prospective implementation for real-time estimation is the following. The flow state at a given time t^* could be estimated by considering the measurements taken at that time and at the previous $N_m - 1$ ones. At the following sampling time, the corresponding new measurements are added and the oldest ones are dropped, keeping the number of measurements considered constant. In other words, reconstruction is carried out using a fixed number of measurements distributed in a time interval which is located before t^*, and which translates as time increases. The sampling rate (i.e. $\tau_m - \tau_{m-1}$) and N_m can be tuned in order to decrease the computational costs while granting the level of accu-

racy required by the particular application. Moreover, when a new set of measurements is added, the Newton method for solving the non-linear system would be restarted from the previous solution, which is already close to the final solution, thus definitely reducing the number of iterations for convergence. In contrast with the other methods, the proposed approaches need a working Galerkin model as a fundamental ingredient. The construction of such a model can be carried out from the information needed to build the POD database, a necessary step for all the methods considered here. Therefore no additional information is needed as compared to other approaches. Moreover, when using the calibration method M2, the cost of building such a model is negligible.

4. Results and discussion

The K-LSQ and K-LSE are used to reconstruct the flow in the configuration described in Section 2, both in the two- ($Re = 150$) and three-dimensional ($Re = 300$) cases. Results are compared to those obtained by the most common techniques available in the literature and reviewed in the Introduction.

Accuracy in the prediction of the single modal coefficients and in the reconstruction of the velocity fields was evaluated. In both cases, differences with respect to the reference case (DNS) were quantified in terms of relative error in the L^2 norm, i.e., the L^2 norm of the difference between the estimated and the reference quantity divided by the norm of the reference quantity.

Several parameters are involved in the set-up of the K-LSQ and K-LSE models. They are related to (i) the dynamic POD model: number of retained modes, calibration interval, number and temporal distribution of available snapshots; (ii) the selected flow measurements: number, type and collocation.

As for the flow measurements, both velocity and shear-stress sensors were used. While velocity measurements are often considered in the literature, due to their widespread use in practice, shear-stress sensors are less common. Nevertheless, they were used here mainly because they are challenging from a numerical point of view, as they involve spatial derivatives of the POD modes. Also, they can be implemented in practice although limitations of accuracy and time resolution may exist (see, for instance, [22]). Different sensor locations were tested, to account for the sensitivity of the proposed approaches to sensor placement. Since the performance of the standard techniques such as LSE or LSQ is influenced by sensor placement, some sensor configurations were selected following the suggestions given for LSE in [8]. On the other hand, none of the considered sensor configurations is optimized for K-LSE or K-LSQ, in order to verify the sensitivity of such methods with respect to sensor placement. In fact, optimal sensor placement may turn out to be a time-consuming operation for complex three-dimensional flows.

4.1. Two-dimensional case: $Re = 150$

The low-order model of the two-dimensional flow is obtained using 95 snapshots, uniformly distributed throughout two vortex-shedding cycles ($T \simeq 13$ is the non-dimensional duration of the time interval), and by retaining $N_r = 6$ modes. The calibration of the model is performed in the same interval using 81 collocation points with method M1. As shown in [12], the calibrated model accurately reproduces the flow inside and outside the calibration interval.

For this rather simple flow, we consider the situation in which a limited number of measurements are available, i.e. only two sensors. Three different configurations were analyzed, two involving streamwise velocity sensors and one involving shear-stress sensors.

The velocity sensors were placed in relation to the spatial structure of the streamwise component of the first two POD modes. In particular, in the first configuration one streamwise velocity sensor is placed on the maximum of the first POD mode which is closest to the cylinder (P1 $\simeq (2.39, 0.52)$) and one in the middle, between P1 and the minimum of the second POD mode closest to the cylinder ($\simeq (1.96, 0.50)$). The second configuration has the first streamwise velocity sensor in P1 and the second one at point (1.98, −0.76). A third configuration was considered with two shear-stress sensors located on the confining walls ($y = \pm 4.0$) at $x = 4$, in a region which satisfies the following criteria on a shedding cycle: the rms value of the shear-stresses is maximum and the reconstruction error of the shear-stresses is minimum for a given number of POD modes.

The parameter C_R in the formulation of the K-LSQ and K-LSE approaches (see Eq. (10)) is set equal to 1. It has been checked that the results do not significantly change if it varies in a neighborhood of this value.

The errors in the prediction of the modal coefficients given by LSQ, LSE, QSE, K-LSQ and K-LSE in the first (velocity sensors) and third (shear-stress sensors) configurations are reported in Tables 1(a) and (b), respectively. The values obtained for the second considered sensor configuration are not shown since they are very similar to those of the first one.

The time interval over which reconstruction is performed is approximately 13 time-units long (non-dimensional time); it contains two shedding cycles, and it starts just after the end of the time interval on which the POD model was built and calibrated.

Tables 2(a) and (b) show the relative reconstruction errors on the velocity components and on their fluctuating part. It appears that two (velocity or shear-stress) sensors are not sufficient to obtain reliable predictions of the modal coefficients by LSQ or LSE. Accuracy problems persist also with the QSE approach, even if in this case the predictions are more accurate than those obtained with LSQ or LSE.

This leads to severe errors in the estimation of the fluctuating part of the velocity field since the first two POD modes represent about 94.8% of the fluctuating energy. Even if the mean flow energy is important with respect to the fluctuating energy, errors in the modal coefficients lead to detectable errors in the reconstruction

Table 1
Relative percentage errors (in L^2 norm) on the estimation of the POD modal coefficients ($e(a_i)$) in the first (a) and third (b) sensor configuration

	$e(a_1)\%$	$e(a_2)\%$	$e(a_3)\%$	$e(a_4)\%$	$e(a_5)\%$	$e(a_6)\%$
(a)						
LSQ	36.33	64.75	280.55	265.66	145.31	117.94
LSE	71.06	27.12	99.71	97.97	99.91	99.93
QSE	20.67	13.03	20.66	40.99	91.05	88.01
K-LSQ	0.47	0.55	2.58	2.66	4.65	4.67
K-LSE	0.82	0.76	9.82	9.82	14.98	15.59
(b)						
LSQ	63.61	84.81	109.32	107.17	100.53	101.39
LSE	46.87	91.97	102.83	100.99	101.40	100.21
QSE	33.32	56.00	78.28	41.62	95.31	75.64
K-LSQ	0.06	0.09	6.06	6.09	9.72	9.56
K-LSE	2.99	3.08	7.07	8.31	17.99	18.47

In this case time-averaging is carried out over the estimation time period.

Table 2
Relative percentage errors (in L^2 norm) on the estimation of the velocity components ($\overline{e(U)}$,$\overline{e(V)}$) and of their fluctuating part ($\overline{e(U')}$, $\overline{e(V')}$), in the first (a) and third (b) sensor configuration

	$\overline{e(U)}\%$	$\overline{e(V)}\%$	$\overline{e(U')}\%$	$\overline{e(V')}\%$
(a)				
LSQ	10.31	57.49	72.15	65.88
LSE	6.32	37.14	53.96	54.26
QSE	2.41	16.06	20.65	23.45
K-LSQ	0.63	3.97	5.39	5.80
K-LSE	0.69	4.42	5.93	6.46
(b)				
LSQ	10.60	64.57	74.31	73.82
LSE	8.05	46.14	68.32	67.44
QSE	4.70	28.28	39.81	41.37
K-LSQ	0.65	4.10	5.54	6.00
K-LSE	0.77	4.91	6.54	7.17

In this case time-averaging is carried out over the estimation time period.

of the velocity components. Note that the reconstruction errors on the vertical component are larger than those on the streamwise one. This is simply because the contribution of the mean flow on the vertical component is much lower than on the streamwise component. Tables 1 and 2 show that both K-LSQ and K-LSE give an accurate estimation not only of the first two modal coefficients, but of all the retained modes. This leads to a precise estimation of the velocity field as well as of its fluctuating part. Moreover, the accuracy of the results is very similar, whether using shear-stress or velocity sensors, indicating a weak sensitivity of the approach to the type and location of the sensors. This is not the case for the LSQ, LSE and QSE methods, which show a higher sensitivity to these aspects, confirming what has already been reported in the literature. When the number of sensor increases, the difference between static and dynamic estimations tend to reduce, as they both tend to the correct values of the Galerkin coefficients.

We compare our results to those of [8], Table 2(a) 13th case. With LSE and two sensors they found $e(a_1) \simeq 76.6\%$ and $e(a_2) \simeq 15.1\%$, errors that are similar to those reported in Table 1(a) for LSE. Using the dynamic estimation, the errors on the same coefficients are two orders of magnitude lower. Furthermore, using the K-LSQ method and two shear-stress sensors (Table 1(b)) the first two modal coefficients are estimated with an error lower than 0.1%, i.e., three orders of magnitude lower than LSE. The estimation results relative to K-LSQ and K-LSE are practically identical if the low-order models are built either by M1 or M2.

The computational times are basically negligible for all cases: the static estimations are accomplished within a fraction of a second (0.0003 s for LSE on a standard personal computer), whereas the dynamic estimations take a longer but still very small time (K-LSQ: 0.6 s, K-LSE: 0.3 s on the same computer).

4.2. Three-dimensional case: $Re = 300$

The flow patterns in this case are definitely more complex than those in the previous one (see [5]).

Two low-order models of the developed three-dimensional flow were derived retaining the first 20 or 60 POD modes obtained from a database of 151 snapshots, uniformly distributed over eight vortex-shedding cycles ($\simeq$ 52 non-dimensional time units from 360 to 412). Calibration was carried out in the same time interval using method M2 (see Section 2). The results obtained by integrating the dynamic model within the calibration interval are reported in Figs. 2 and 3, in which the calibrated POD coefficients are compared to those obtained from the projection of the fully resolved Navier–Stokes simulations. A comparison between the

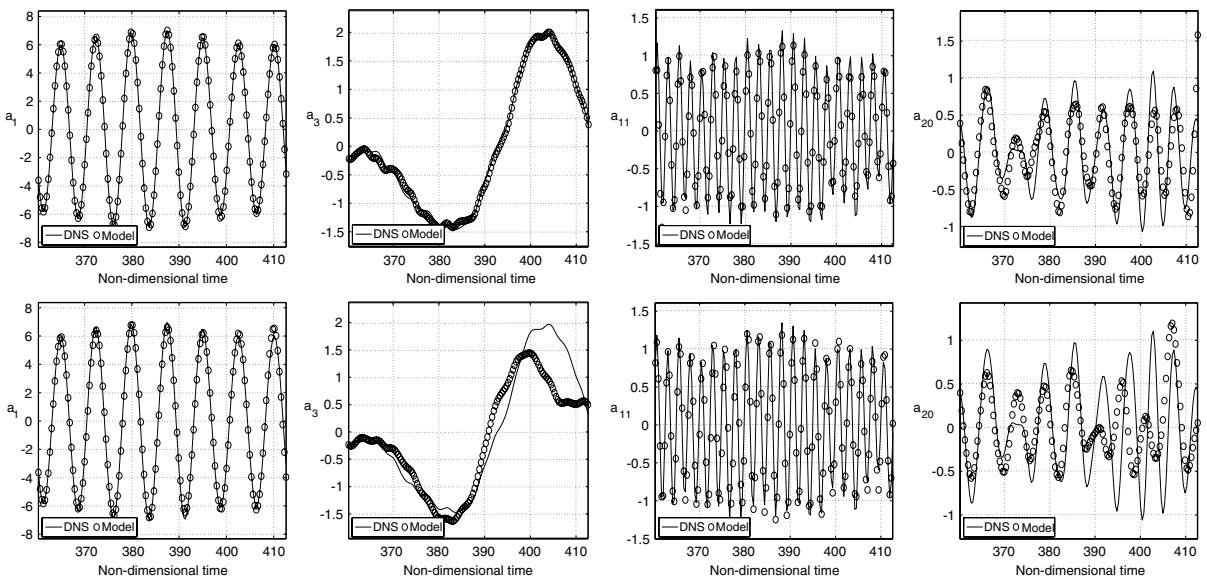

Fig. 2. Three-dimensional flow: projection of the fully resolved Navier–Stokes simulations over the POD modes (continuous line) vs. the integration of the dynamical system inside the calibration interval, obtained retaining the first 20 POD modes (circles). The first row is relative to M1, the other to M2. Only some representative coefficients are shown.

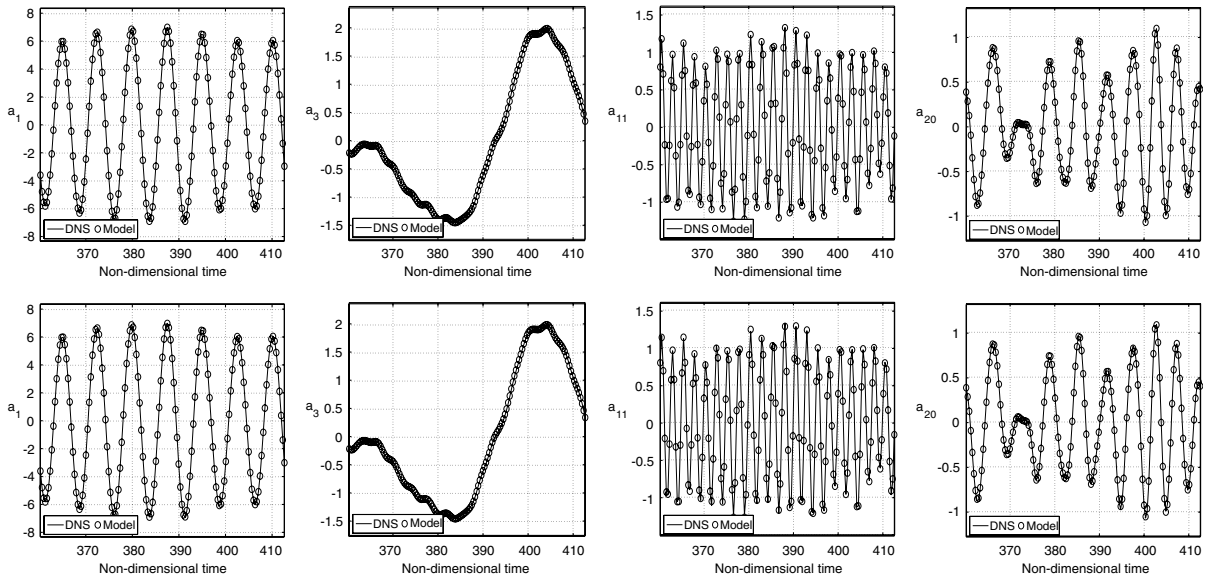

Fig. 3. Three-dimensional flow: projection of the fully resolved Navier–Stokes simulations over the POD modes (continuous line) vs. the integration of the dynamical system inside the calibration interval, obtained retaining the first 60 POD modes (circles). The first row is relative to M1, the other to M2. Only some representative coefficients are shown.

results obtained using the two different calibration techniques (M1 and M2) is also provided. Model M1 is of course more accurate, although the differences become almost negligible as the number of modes retained increases. In both cases, the POD model shows a good accuracy inside the calibration interval. However, in the three-dimensional case, these results tend to deteriorate outside the time interval in which the calibration is performed, as shown in the following. Furthermore, we analyze the ability of the retained POD modes to represent the flow field in the interval in which the flow estimation is carried out. This time interval begins about 82 time units after the end of the calibration interval (at time 494), and is approximately 30 time units long, including approximately four shedding cycles. In Table 3 we give the minimum error that we can hope to achieve when reconstructing the fluctuating part of the velocity components. The minimum error corresponds to the case where the estimated POD coefficients coincide with those obtained by projecting the reference Navier–Stokes solution over the POD modes, i.e., $\bar{\alpha}_i(t) = \alpha_i(t)$. This error is computed over the entire domain, and over a subset defined by $0 \leqslant x/L \leqslant 6$, which corresponds to the near wake of the cylinder. These errors are not small, even if we increase the number of modes from 20 to 60, as shown in Table 3. In fact, using a larger number of POD modes does not help in general. Using 60 modes instead of 20 does not reduce significantly the representation error because the modes from 20 to 60 are not statistically relevant outside the reference interval where the snapshots were taken. In other words, in order to increase the representativeness of those modes (20–60) outside the reference interval one should take larger databases encompassing longer time lags. However, the problem is that the convergence rate of the POD modes with respect to the number of snapshots included in the database is very low. In this case, for example, using 60 modes, the relative approximation

Table 3
Minimum errors on the fluctuating part of the velocity components

	$\overline{e(U'_{ent})}\%$	$\overline{e(V'_{ent})}\%$	$\overline{e(W'_{ent})}\%$	$\overline{e(U'_{06})}\%$	$\overline{e(V'_{06})}\%$	$\overline{e(W'_{06})}\%$
20 modes	57.48	43.41	95.57	47.27	43.21	99.37
60 modes	56.78	41.76	94.72	46.34	41.21	98.77

Twenty and 60 POD modes, over the entire flow field (*ent*) and over the near wake (06). The time interval considered is 82 non-dimensional time units (about 10 shedding cycles) away from the time interval where the POD modes were derived.

error goes down from 40% to 30% when the database goes from 151 snapshots to 912 snapshots, that is the limit of our computational resources.

The largest errors are on the span-wise component, since the retained POD modes poorly represent this component of the velocity as it is not energetically significant, in average, with respect to the remaining ones. This aspect might be improved working on the construction of the POD basis choosing, for instance, a different norm which gives more weight to the span-wise component of the velocity or which corresponds to a quantity different from kinetic energy.

In other words, the accuracy of the best possible reconstruction is limited from above by the capability of the POD modes to actually represent the flow outside the time interval where the snapshots were taken, which however, increases using a larger snapshots database, as shown in [5]. Note, however, that this problem is common to all the considered reconstruction techniques, since they all use the POD representation of the velocity field. Because of the complexity of the flow, more measurements were used for the reconstruction procedure, organized in five different configurations, two involving only velocity measurements and three involving both velocity and shear-stress measurements. In the last three configurations, the shear-stress sensors were selected following the same criterion adopted in the 2D case, they are 14 in number and in all considered cases are symmetrically placed on both the confining walls ($y = \pm 4$) at $x = 4$ and $z = \{1.2, 1.5, 2.7, 3, 3.3, 4.5, 4.8\}$. The placement of the velocity sensors has again been chosen on the basis of the spatial structure of the streamwise velocity of the first 12 POD modes. The different configurations are listed below, together with a brief description of the rationale for the placement of the velocity sensors:

Table 4
Positions of the velocity sensors in the three-dimensional case, configuration (e)

Velocity sensor	x	y	z
1	5.02	0.96	2.00
2	7.00	0.96	2.00
3	6.01	−0.96	2.00
4	6.01	0.96	4.00
5	5.02	−0.96	4.00
6	7.00	−0.96	4.00

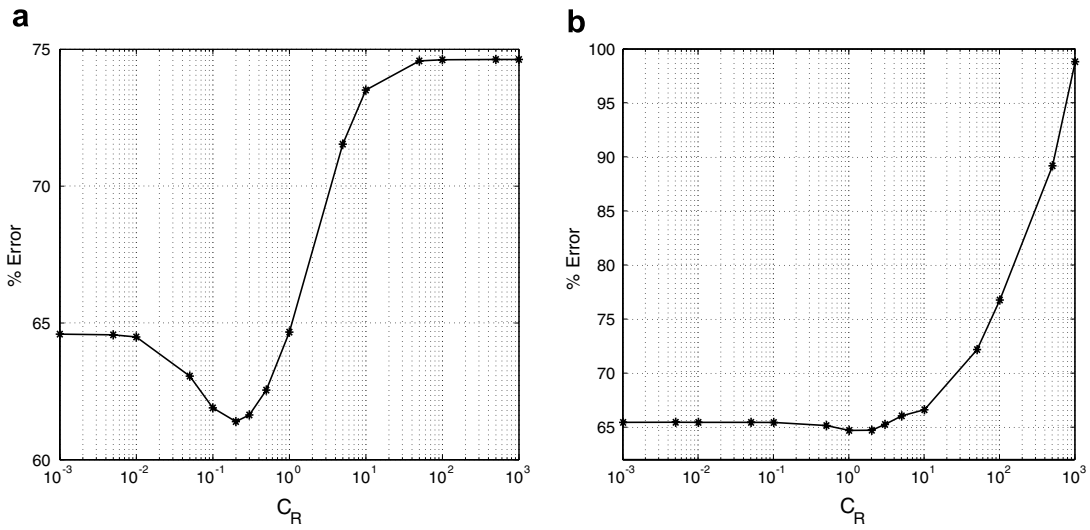

Fig. 4. Relative percent error in the reconstruction of the fluctuating U component, when varying C_R: (a) KLSE; (b) KLSQ.

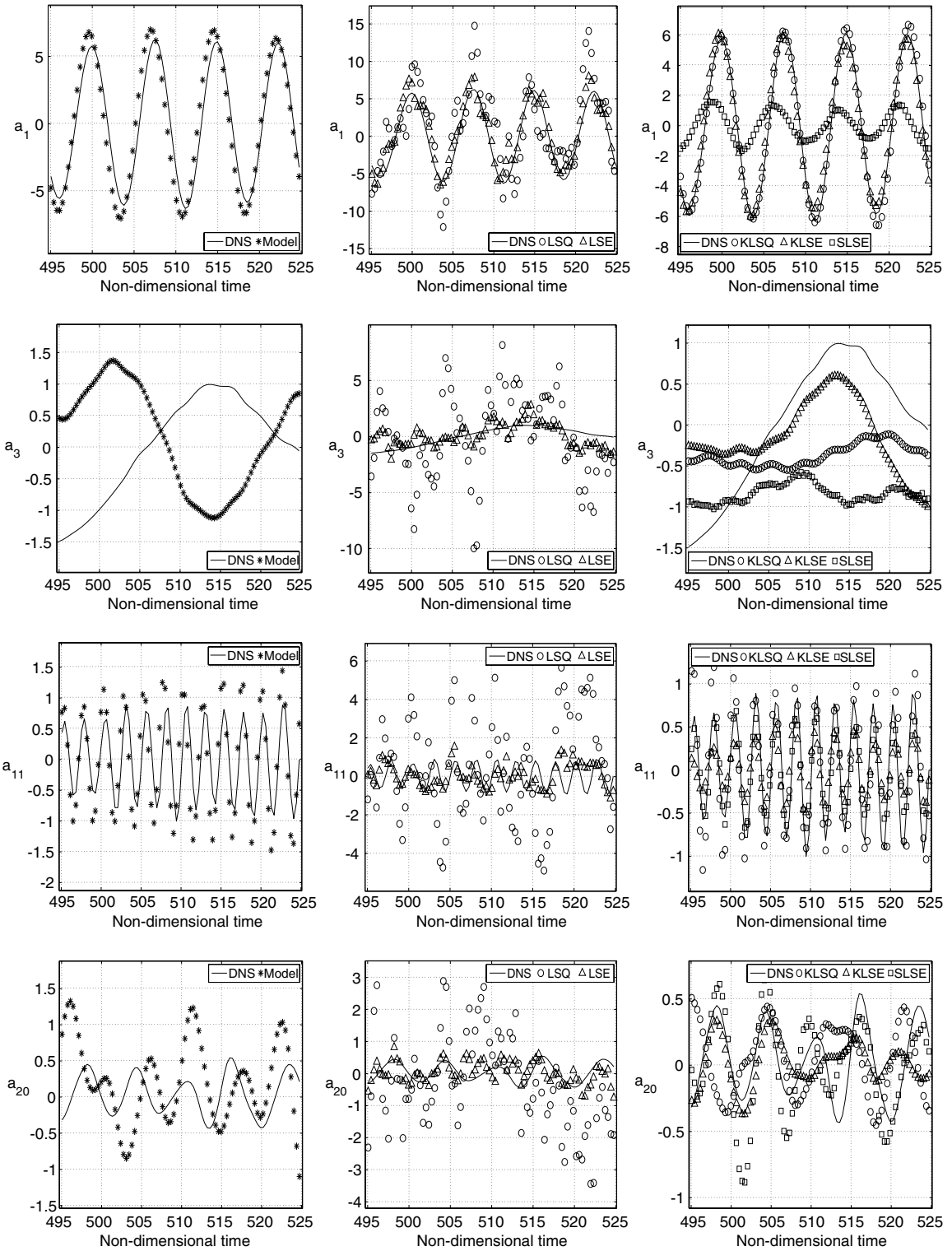

Fig. 5. Estimation of some representative modal coefficients in the three-dimensional case, for sensor configuration (b) and far from the calibration interval, together with the reference values evaluated from the DNS simulation. Note that the same graph is reported in the three columns but the axis scales are different. Model M2 with 20 modes.

(a) Twenty four velocity sensors distributed on six equispaced slices in the axial (z) direction; on each slice, the sensors are on the lines connecting the maximum and minimum, closest to the cylinder, of the first two POD modes. On each segment, the sensors are approximately in the middle, but slightly closer to the extrema of the first POD mode.
(b) Twenty four velocity sensors distributed on four equispaced slices in the axial (z) direction; on each slice, three points are selected in the region of overlapping between the maxima and minima of the low-frequency POD modes (modes 3, 4, 7, 8, 9 and 10) and three on the overlapping region of the extrema of the vortex-shedding modes (modes 1, 2, 5, 6, 7, 11 and 12) (see [5] for details on the separation between low-frequency and vortex-shedding POD modes).
(c) Fourteen shear-stress sensors and 10 velocity sensors distributed on five equispaced slices in the axial (z) direction; on each slice, the velocity sensors are placed on the maximum and minimum closest to the cylinder of the first POD mode.
(d) Fourteen shear-stress sensors and 10 velocity sensors. Six equispaced slices in the axial (z) direction are considered. On four slices, two velocity sensors are placed as in the previous case. Two sensors are placed on the remaining slices, corresponding respectively to the maximum and minimum of the third POD mode (low frequency mode).
(e) Fourteen shear-stress sensors and six velocity sensors located in the wake, at the points reported in Table 4.

The parameter C_R of Eq. (10) was selected by experimenting with different values. For example, in Fig. 4(a), we show the L^2 relative error for the reconstruction by K-LSE of the fluctuating U component, as a function of C_R. The results are relative to configuration (b). The plotted curve shows a minimum for $C_R = 0.2$ and therefore in the following we chose $C_R = 0.2$ for K-LSE. Note that for $C_R \geqslant 10^2$ the results are basically those of a simple LSE. A similar analysis was performed using K-LSQ (see Fig. 4(b)) and the best value that was selected is $C_R = 1$.

Results relative to configuration (b) are reported in Fig. 5, where some representative modal coefficients predicted by the calibrated POD model M2 with 20 modes, LSQ, LSE, K-LSQ, K-LSE and SLSE are plotted, together with the projection of the DNS velocity fields on the corresponding POD mode. Results for configuration (b) are shown because the sensor placement is appropriate for the LSE method, as already discussed, and this makes the comparison with the proposed approaches more comprehensive.

In Fig. 5, left column, one can observe that, in contrast with the two-dimensional case and as previously stated, the POD model is less accurate outside the calibration interval. However, long after the end of the calibration interval, the model remains stable, and the error bounded. The results obtained with the other sensor configurations or with model M1 are similar to those reported in Fig. 5, except for LSE and LSQ methods which are less accurate as they are more sensitive to sensor placement. In Fig. 5 it is seen that LSE and LSQ, provide reasonable predictions only for the first two modal coefficients, that are associated with the vortex-shedding dynamics. The second modal coefficient, not shown in the Figure, is identical to the first one except for a phase shift of $\pi/2$ in time. However, the results in terms of approximation are the same. The predictions of the remaining modes are completely unreliable. When dynamic estimation is applied, or when the

Table 5
Reconstruction errors obtained with model M2 and 20 modes for sensor configurations (a) and (b)

	$\overline{e(U'_{ent})}\%$	$\overline{e(V'_{ent})}\%$	$\overline{e(W'_{ent})}\%$	$\overline{e(U'_{06})}\%$	$\overline{e(V'_{06})}\%$	$\overline{e(W'_{06})}\%$
SC (a)						
KLSQ	63.54	49.77	101.11	48.78	44.92	106.65
KLSE	62.63	48.37	100.95	47.22	44.26	101.71
SLSE	66.39	49.12	104.92	49.77	46.59	110.60
SC (b)						
KLSQ	64.67	49.77	102.26	49.94	48.35	108.64
KLSE	61.40	47.03	98.45	47.17	43.73	101.09
SLSE	95.77	91.14	110.56	91.15	89.14	112.42

Errors computed on the entire domain (*ent*) and in the near wake (06).

SLSE approach is used, predictions are definitely improved. In particular, this is true for modes like a_1 or a_{11} that are related to the vortex-shedding, i.e., almost periodic with a period that is the same or a multiple of the vortex-shedding period. The prediction of the remaining modes is less accurate (see a_3 and a_{20}), especially when very low frequencies are dominant, as in the case of a_3. However, the overall accuracy is significantly

Table 6
Reconstruction errors obtained with model M2 and 20 modes for sensor configurations (c), (d) and (e)

	$\overline{e(U'_{ent})}\%$	$\overline{e(V'_{ent})}\%$	$\overline{e(W'_{ent})}\%$	$\overline{e(U'_{06})}\%$	$\overline{e(V'_{06})}\%$	$\overline{e(W'_{06})}\%$
SC (c)						
KLSQ	62.68	48.72	100.00	48.53	45.54	103.87
KLSE	66.76	51.78	99.42	53.94	51.87	103.85
SLSE	76.01	56.46	112.81	53.60	52.72	118.65
SC (d)						
KLSQ	67.54	53.44	104.86	52.16	48.86	111.07
KLSE	64.35	51.14	101.01	52.06	50.58	105.30
SLSE	70.95	55.75	108.64	55.24	55.30	116.96
SC (e)						
KLSQ	132.40	97.56	162.68	96.73	100.01	183.59
KLSE	64.37	49.63	99.49	52.10	50.20	103.12
SLSE	79.12	58.98	115.97	57.16	55.15	124.96

Errors computed on the entire domain (*ent*) and in the near wake (06).

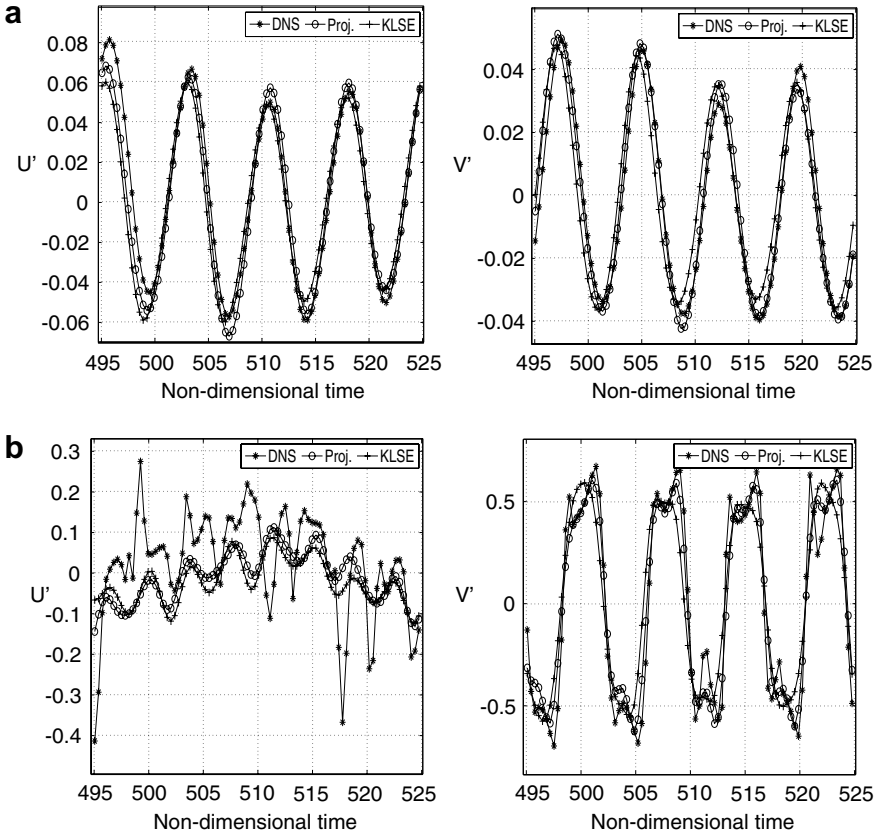

Fig. 6. Reconstruction of U' and V' components of the velocity at points: (a) $x/L = 2.55, y/L = 2.51, z/L = 3.00$; (b) $x/L = 5.45, y/L = 0.00, z/L = 3.00$.

improved in comparison with the LSQ and LSE approaches alone. The static estimations are accomplished within a fraction of a second (0.0012 s for LSE), whereas the dynamic estimations still take less than a minute (K-LSQ: 21 s, K-LSE: 25 s).

In Tables 5 and 6, the actual errors obtained using 20 modes are given. The errors of LSE and LSQ are not included since they are larger than the others. We observe that the dynamic approaches are systematically more accurate than SLSE and that the reconstruction errors can be considered satisfactory as they are close to the minimum error possible (see Table 3). Furthermore the reconstruction errors progressively increase

Table 7
Comparison between reconstruction errors obtained with model M2 and 20 or 60 modes for sensor configuration (b)

SC (b)	$\overline{e(U'_{ent})}\%$	$\overline{e(V'_{ent})}\%$	$\overline{e(W'_{ent})}\%$	$\overline{e(U'_{06})}\%$	$\overline{e(V'_{06})}\%$	$\overline{e(W'_{06})}\%$
KLSE 20 M	61.40	47.03	98.45	47.17	43.73	101.09
KLSE 60 M	61.37	46.70	98.65	46.93	42.85	100.77

Errors computed on the entire domain and in the near wake.

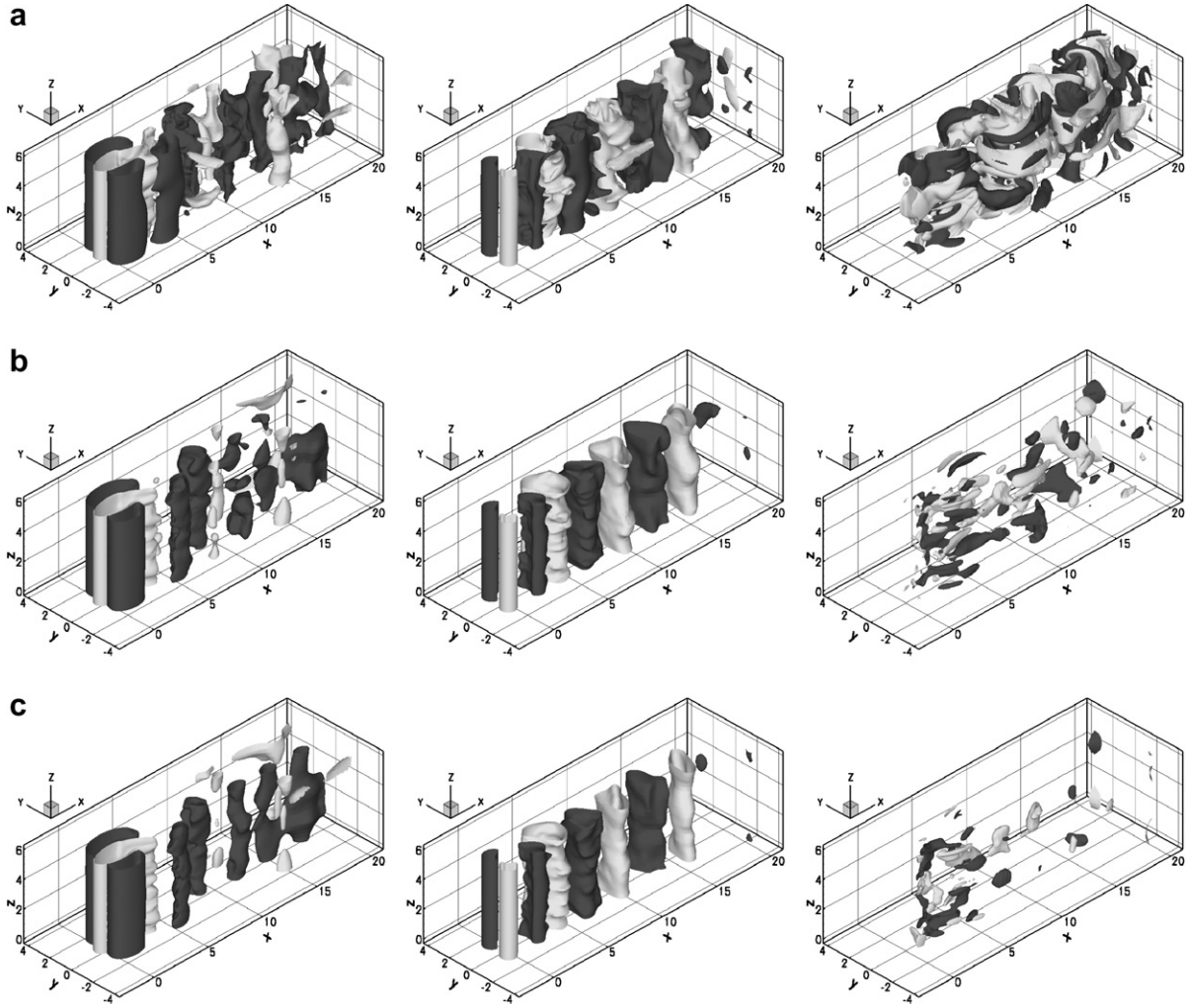

Fig. 7. Isosurfaces of the velocity components u (left, grey = 0.5, dark grey = 1.0), v (center, grey = −0.25, dark grey = 0.25) and w (right, grey = −0.075, dark grey = 0.075) of a snapshot outside the database: (a) actual snapshot; (b) snapshot projected on the retained POD modes; (c) reconstructed snapshot using the K-LSE technique with the sensor configuration (b).

moving away from the cylinder in the downstream direction. Concerning the span-wise component of the velocity, as previously discussed, errors are large since the retained POD modes themselves poorly represent this component of velocity (see Tables 5 and 6).

As an example of an actual estimation in the physical space, we considered two points located on the symmetry plane orthogonal to the span-wise direction. They were selected in order to represent the typical results obtained. In Fig. 6 we show the actual U' and V' components of the velocity obtained by DNS, the projection on the POD basis as well as the estimation obtained by K-LSE, using M2, 20 POD modes and sensor configuration (b). We observe that the estimation is accurate for the point in the wake where the time evolution is smooth. At the other point, located on the horizontal axis in a region where highly three-dimensional phenomena take place, we observe sudden bursts of activity that are filtered away by the estimation, at least for the U component.

The K-LSQ, K-LSE and SLSE methods are similar in the sensitivity of the predictions to sensors type and placement, which is generally low. Nevertheless, the predictions given by the K-LSE method are systematically the most insensitive to sensor placement. Table 7 compares the results obtained with 20 modes and those obtained with 60 modes, using model M2 and sensor configuration (b). A slight improvement of the estimation can be observed. The same conclusion applies for the other sensor configurations not reported here. Using model M1 the results are basically the same as those shown here.

In Fig. 7 the velocity components obtained by DNS at $t = 426.6$ (a snapshot outside the database used for the construction and calibration of the POD model) are plotted together with their projections on the space of the retained POD modes. These projections represent the best approximation of the flow which can be estimated with the retained POD modes, and with the prediction given by the K-LSE method. It can be seen that the main structures characterizing the streamwise and lateral velocity fields are well reconstructed. As for the span-wise velocity component, the reconstruction accuracy is not satisfactory, but this is due to the fact that it is one order of magnitude lower than the other components, as already discussed.

5. Conclusions

We devised a method to build a non-linear observer for unsteady flows. This method is based on the coupling of a non-linear low-dimensional model of the flow with a linear technique that estimates the coefficients of the flow representation in terms of POD modes. The underlying idea is that the estimated flow should approximately satisfy the POD model. The coupling leads to a non-linear minimization problem solved by a pseudo-spectral approach and a Newton method.

The non-linear observer was applied to the laminar flow around a confined square cylinder at two different Reynolds numbers; for the first the flow is two-dimensional, while in the second case complicated three-dimensional phenomena occur in the wake.

In the two-dimensional case, with a limited number of sensors, the proposed procedure is able to give a significantly more accurate estimation of the POD coefficients and of the whole velocity field than the LSQ, LSE and QSE approaches.

In the three-dimensional case, the flow dynamics are more complex, and not only LSE and LSQ, but also the calibrated POD dynamical system provide poor coefficient estimations when used outside the calibration interval. Conversely, the proposed procedure, combined with either LSQ or LSE, gives satisfactory predictions of the coefficients of those POD modes that are related to vortex-shedding. For the remaining modes, the accuracy is lower. Nevertheless, the instantaneous velocity fields are reconstructed with an accuracy close to the best possible, which is the one that would be obtained by projecting the DNS fields on the retained POD modes.

Moreover, K-LSE and K-LSQ methods are weakly sensitive to sensor type and placement. The results obtained with the proposed approaches are comparable to those obtained by the SLSE approach, which also uses the temporal history of the flow measurements, but in the Fourier space. This latter technique has a computational complexity which is significantly larger than that of LSE or LSQ, and comparable to that of the proposed approaches.

From the present study, it appears that, probably, for flows characterized by complex dynamics, the major limitation of all estimation techniques based on POD is indeed the ability of the retained POD modes to adequately representing the flow field.

Thus, one way to improve the present results for the three-dimensional case is to include statistical information concerning the errors both in the model and in the measured quantities, since the POD modes do not give an accurate representation of the flow field. Including the parameter C_R in the formulation is indeed a rudimental approach that shows the influence of the relative weight given to the model or the measurements.

Another way is obviously to build a more accurate POD model. A possibility is to take larger data bases to compute POD modes having better approximation properties. However, this may not be pushed too far because of the huge amount of computational resources required for managing large DNS datasets. Another promising approach in this direction could be to modify the scalar product used in the definition of the POD modes in such a way as to take into account the most observable events in the flow.

Acknowledgment

This work was funded in part by the HPC-EUROPA project (RII3-CT-2003-506079). IDRIS (Orsay, France) and M3PEC (Université Bordeaux 1, France) provided the computational resources.

References

[1] H.D.I. Abarbanel, R. Brown, J.J. Sidorowich, L.S. Tsimring, The analysis of observed chaotic data in physical systems, Reviews of Modern Physics 65 (4) (1993) 1331–1392.
[2] R.J. Adrian, On the role of conditional averages in turbulent theory, in: G. Patteson, J. Zakin (Eds.), Turbulence in Liquids: Proceedings of the fourth Biennial Symposium on Turbulence in Liquids, Science Press, Princeton, 1977, pp. 322–332.
[3] V. Akcelik, J.Bielak, G. Biros, I. Epanomeritakis, A. Fernandez, O. Ghattas, E.J. Kim, J. Lopez, D. O'Hallaron, T. Tu, J. Urbanic, High-resolution forward and inverse earthquake modeling on terascale computers, in: Proceedings of ACM/IEEE SC2003 Phoenix, AZ, 2003.
[4] J. Bonnet, D. Cole, J. Delville, M. Glauser, L. Ukeiley, Stochastic estimation and proper orthogonal decomposition: complementary techniques for identifying structures, Experiments in Fluids 17 (1994) 307–314.
[5] M. Buffoni, S. Camarri, A. Iollo, M. Salvetti, Low-dimensional modelling of a confined three-dimensional wake flow, Journal of Fluid Mechanics 569 (2006) 141–150.
[6] S. Camarri, F. Giannetti, On the inversion of the Kármán street in the wake of a confined square cylinder, Journal of Fluid Mechanics 574 (2007) 169–178.
[7] K. Cohen, S. Siegel, T. McLaughlin, A heuristic approach to effective sensor placement for modeling of a cylinder wake, Computers and Fluids 35 (2006) 103–120.
[8] K. Cohen, S. Siegel, D. Wetlesen, J. Cameron, A. Sick, Effective sensor placements for the estimation of proper orthogonal decomposition mode coefficients in von Kármán vortex street, Journal of Vibration Control 10 (2004) 1857–1880.
[9] R. Everson, L. Sirovich, Karhunen–Loeve procedure for gappy data, Journal of the Optical Society of America A 12 (8) (1995) 1657–1664.
[10] D. Ewing, J. Citriniti, Examination of a LSE/POD complementary technique using single and multi-time information in the axisymmetric shear layer, in: J.N. Sorensen, E.J. Hopfinger, N. Aubry (Eds.), Proceedings of the IUTAM Symposium on Simulation and Identification of Organized Structures in Flows, Fluid Mechanics and its Applications, vol. 52, Springer, 1999, pp. 375–384.
[11] B. Galletti, A. Bottaro, C. Bruneau, A. Iollo, Accurate model reduction of transient flows, European Journal of Mechanics B: Fluids 26 (2007) 354–366.
[12] B. Galletti, C.H. Bruneau, L. Zannetti, A. Iollo, Low-order modelling of laminar flow regimes past a confined square cylinder, Journal of Fluid Mechanics 503 (2004) 161–170.
[13] J. Hoepffner, M. Chevalier, T. Bewley, D. Henningson, State estimation in wall-bounded flow systems. Part 1. Perturbed laminar flows, Journal of Fluid Mechanics 534 (2005) 263–294.
[14] R.E. Kalman, A new approach to linear filtering and prediction problems, Transactions of the ASME – Journal of Basic Engineering 82 (Series D) (1960) 35–45.
[15] F. Le Dimet, O. Talagrand, Variational algorithms for analysis and assimilation of meteorological observations: theoretical aspects, Tellus A 38 (1986) 97–110.
[16] J.-L. Lions, Contrôle Optimale de Systèmes Gouvernés par des Équations aux Dérivés Partielles, Dunod-Gauthier-Villars, Paris, 1968.
[17] J.L. Lumley, The structure of inhomogeneous turbulent flows, in: A.M. Yaglom, V.L. Tatarski (Eds.), Atmospheric Turbulence and Radio Wave Propagation, Nauka, Moscow, 1967, pp. 166–178.
[18] X. Ma, G.E. Karniadakis, H. Park, M. Gharib, DPIV-driven flow simulation: a new computational paradigm, Proceedings of the Royal Society A: Mathematical, Physical and Engineering Sciences 459 (2031) (2003) 547–565.
[19] A.M. Naguib, C.E. Wark, O. Juckenhöfel, Stochastic estimation and flow sources associated with surface pressure events in a turbulent boundary layer, Physics of Fluids 13 (2001) 2611–2626.
[20] R. Schmit, M.N. Glauser, Use of low-dimensional methods for wake flow field estimation from dynamic strain, AIAA Journal 43 (5) (2005) 1133–1136.

[21] L. Sirovich, Turbulence and the dynamics of coherent structures. Parts I, II and III, Quarterly of Applied Mathematics XLV (1987) 561–590.
[22] P. Spazzini, G. Iuso, M. Onorato, N. Zurlo, Design, test and validation of a probe for time-resolved measurement of skin friction, Measurement Science and Technology 10 (7) (1999) 631–639.
[23] C. Tinney, F. Coiffet, J. Delville, A. Hall, P. Jordan, M.N. Glauser, On spectral linear stochastic estimation, Experiments in Fluids 41 (5) (2006) 763–775.
[24] D. Venturi, G.E. Karniadakis, Gappy data and reconstruction procedures for flow past a cylinder, Journal of Fluid Mechanics 519 (2004) 315–336.
[25] K. Willcox, Unsteady flow sensing and estimation via the gappy proper orthogonal decomposition, Computers and Fluids 35 (2006) 208–226.